

OPEN ACCESS

Local structure information by EXAFS analysis using two algorithms for Fourier transform calculation

To cite this article: N Aldea *et al* 2009 *J. Phys.: Conf. Ser.* **182** 012056

View the [article online](#) for updates and enhancements.

You may also like

- [Bond compressibility and bond Grüneisen parameters of CdTe](#)
P Fornasini, R Grisenti, T Irifune *et al.*
- [Large negative thermal expansion of the Co subnetwork measured by EXAFS in highly disordered Nd_xCo_{1-x} thin films with perpendicular magnetic anisotropy](#)
J Díaz, R Cid, A Hierro *et al.*
- [Low-dimensional systems investigated by x-ray absorption spectroscopy: a selection of 2D, 1D and 0D cases](#)
Lorenzo Mino, Giovanni Agostini, Elisa Borfecchia *et al.*



ECS
The
Electrochemical
Society
Advancing solid state &
electrochemical science & technology

DISCOVER
how sustainability
intersects with
electrochemistry & solid
state science research

Local structure information by EXAFS analysis using two algorithms for Fourier transform calculation

N Aldea¹, S Pintea¹, V Rednic¹, F Matei², Hu Tiandou³ and Xie Yaning³

¹National Institute for Research and Development of Isotopic and Molecular Technologies, 65-103 Donath, 400293 Cluj-Napoca, Romania

²University of Agricultural Sciences and Veterinary Medicine, 3-5 Calea Manastur, 400372 Cluj-Napoca, Romania

³Beijing Synchrotron Radiation Facilities of Beijing Electron Positron Collider National Laboratory, People's Republic of China

E-mail: nicolae.aldea@itim-cj.ro

Abstract. The present work is a comparison study between different algorithms of Fourier transform for obtaining very accurate local structure results using Extended X-ray Absorption Fine Structure technique. In this paper we focus on the local structural characteristics of supported nickel catalysts and Fe₃O₄ core-shell nanocomposites. The radial distribution function could be efficiently calculated by the fast Fourier transform when the coordination shells are well separated while the Filon quadrature gave remarkable results for close-shell coordination.

1. Introduction

The X-ray absorption spectroscopy (XAS) can yield several characteristic of the studied material: the electronic and structural information about the local environment around a specific atomic constituent in the amorphous materials [1-2], the location and chemical state of any catalytic atom on any support [3] and the nanoparticle size of the transition metal oxides [4-5]. Extended X-ray absorption fine structure (EXAFS) is a scattering technique in which a core electron ejected by an X-ray photon probes the local environment of the absorbing atom. The ejected photoelectron backscattered by the neighboring atoms located around the absorbing atom interferes constructively with the outgoing electron wave depending on its energy. The energy of the photoelectron is equal to the difference between the X-ray photon energy and a threshold energy associated with the ejection of the electron.

2. Theoretical background

The interference between the outgoing and backscattered electron waves has the effect of modulating the X-ray absorption coefficient. The EXAFS function $\chi(k)$ is defined in terms of the atomic absorption coefficient by:

$$\chi(k) = \frac{\mu(k) - \mu_0(k)}{\mu_0(k)} \quad (1)$$

where k is the electron wave vector, $\mu(k)$ refers to the absorption by an atom from the material of interest and $\mu_0(k)$ refers to the absorption by a free atom. Theories of EXAFS based on the single scattering approximation of the ejected photoelectron by atoms in immediate vicinity of the absorbing atom give the following expression for $\chi(k)$ [6]:

$$\chi(k) = \sum_j A_j(k) \sin[2kr_j + \delta_j(k)] \quad (2)$$

where the sum extends over j^{th} coordination shell, r_j is the radial distance from the j^{th} shell and $\delta_j(k)$ is the total phase shift function. The amplitude function $A_j(k)$ is given by:

$$A_j(k) = \left(\frac{N_j}{kr_j^2} \right) F(k, r_j, \pi) \exp[2r_j / \lambda_j(k) - k^2 \sigma_j^2] \quad (3)$$

In this equation N_j is the number of atoms in the j^{th} shell, σ_j is the root means squares deviation of distance about r_j , $F(k, r, \pi)$ is the backscattering amplitude and $\lambda_j(k)$ is the mean free path function for inelastic scattering. The backscattering factor and the phase shift depend on the kind of atom responsible for scattering and its coordination shell [7]. The analysis of EXAFS data for obtaining structural information [N_j , r_j , σ_j , $\lambda(k)$] generally proceeds by employing the Fourier transform. The radial structure function (RSF) can be derived from $\chi(k)$. The single shell may be isolated by Fourier transform:

$$\Phi(r) = \int_{-\infty}^{\infty} k^n \chi(k) WF(k) \exp(-2ikr) dk. \quad (4)$$

The EXAFS signal is weighted by k^n ($n = 1, 2, 3$) to get the distribution function of atom distances. Different apodization windows $WF(k)$ are available as Gauss or Hanning. For experimental reasons it is not possible to cover the full $(-\infty, +\infty)$ wave vector interval. If we take into consideration Δr and Δk as mesh values for variables r and k and we consider N values of k variable, then between meshes Δr and Δk there is following relation:

$$\Delta r = \frac{1}{N\Delta k}. \quad (5)$$

With these assumptions the general relation for discrete Fourier transform is given by

$$\Phi(n\Delta r) = \Delta k \sum_{m=-N/2}^{N/2-1} h(m\Delta k) \exp\left(-\frac{2\pi imn}{N}\right) \quad (6)$$

where $h = k^n \chi WF$ and $n = \overline{0, N-1}$. The fast Fourier transform algorithm [8] was developed based on relation (6) and was successfully used in many applications. Advantages and limits of this algorithm are treated in reference [9]. Beside this algorithm we also implemented in our software package a generalized Filon quadrature [10] for direct and inverse Fourier transform calculation. The following relations give the real and imaginary parts of the Fourier transform:

$$\int_{x_0}^{k_{2n}} h(k) \cos 2\pi kr dk \approx \Delta k [\alpha(2\pi r \Delta k) (h_{2n} \sin 2\pi k_{2n} r - h_0 \sin 2\pi k_0 r) + \beta(2\pi r \Delta k) C_{2n} + \gamma(2\pi r \Delta k) C_{2n-1}] \quad (7)$$

$$\int_{x_0}^{k_{2n}} h(k) \sin 2\pi kr dk \approx \Delta k [\alpha(2\pi r \Delta k) (h_0 \cos 2\pi k_0 r - h_{2n} \cos 2\pi k_{2n} r) + \beta(2\pi r \Delta k) S_{2n} + \gamma(2\pi r \Delta k) S_{2n-1}] \quad (8)$$

where

$$C_{2n} = \sum_{i=0}^n h_{2i} \cos(2\pi k_{2i}) - \frac{1}{2} [h_{2n} \cos 2\pi k_{2n} + h_0 \cos 2\pi k_0], \quad C_{2n-1} = \sum_{i=1}^n h_{2i-1} \sin 2\pi k_{2i-1},$$

$$S_{2n} = \sum_{i=0}^n h_{2i} \sin(2\pi k_{2i}) - \frac{1}{2} [h_{2n} \sin(2\pi k_{2n}) - h_0 \sin(2\pi k_0)], \quad S_{2n-1} = \sum_{i=1}^n h_{2i-1} \sin(2\pi k_{2i-1})$$

$$\alpha(\theta) = \frac{1}{\theta} + \frac{\sin 2\theta}{2\theta^2} - \frac{2\sin^2 \theta}{\theta^3}, \quad \beta(\theta) = 2 \left(\frac{1 + \cos^2 \theta}{\theta^2} - \frac{\sin 2\theta}{\theta^3} \right), \quad \gamma(\theta) = 4 \left(\frac{\sin \theta}{\theta^3} - \frac{\cos \theta}{\theta^2} \right).$$

If $0 < \theta < 1$, functions α, β and γ can be successfully approximated by:

$$\alpha \approx \frac{2\theta^3}{45} - \frac{2\theta^5}{315} + \frac{2\theta^7}{4725}, \quad \beta \approx \frac{2}{3} + \frac{2\theta^2}{15} - \frac{4\theta^4}{105} + \frac{2\theta^6}{567}, \quad \gamma \approx \frac{4}{3} - \frac{2\theta^2}{15} + \frac{\theta^4}{210} - \frac{\theta^6}{11340}.$$

3. Experimental

The transmission EXAFS measurements were carried out in the 4W1B beamlines at the Beijing Synchrotron Radiation Facilities (BSRF) operating at 50-80 mA and 2.2 GeV at room temperature. The features of 4W1B beamline are: energy range of 3.5-22 keV, energy resolution of $\Delta E = 0.5-2$ eV at $E = 10$ keV, Bragg angle range of $5-70^\circ$, the crystals Si(111), Si(220) and Si(311) can be alternatively used. Fe_3O_4 powders with 99.98% purity and Ni nanoclusters supported on Cr_2O_3 treated at 350°C were used as test samples. Atomic concentration of Ni and Cr were 85%, respectively 15at%. Harmonics were rejected by detuning of monochromator. Absorption coefficients of Fe and Ni K edges were determined using a Si(111) double-crystal monochromator. Ionization chambers monitored the X-ray intensities of incident and transmitted beams. Special care was taken in sample preparation, especially for the thickness and homogeneity of the samples, in order to obtain high quality absorption spectra. All samples were ground to fine powder and homogeneously dusted on scotch tape. We used for absorption coefficients measurements, the energy scanning range from 6994 eV to 8108 eV and 8200 eV to 9300 eV for Fe_3O_4 and Ni/ Cr_2O_3 nanosystems, respectively. The EXAFS analysis of the absorption coefficients was processed with computer codes EXAFS51 to EXAFS56 [11] from our library.

4. Results and discussion

The structure of Fe_3O_4 nanoclusters is an interesting problem from EXAFS perspective because it involves three types of absorbers: the tetrahedral Fe^{3+} , the octahedral Fe^{3+} and octahedral Fe^{2+} .

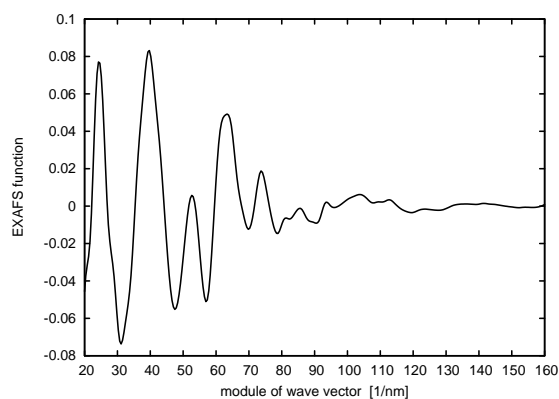


Figure 1. The EXAFS signal of Fe K edge for investigated sample.

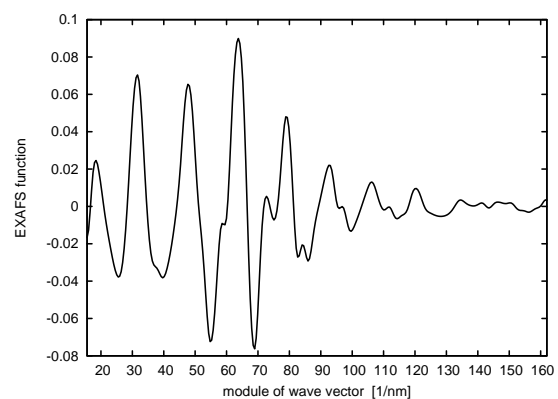


Figure 2. The EXAFS signal of Ni K edge for investigated sample.

The extraction of EXAFS signals requires several steps: calculation of the threshold energy of Fe and Ni K-edges, background removal through pre-edge and after-edge base line fitting with different possible modelling functions, and $\mu_0(k)$ and $\mu(k)$ evaluation. In accordance with equation (1) EXAFS signals were processed for intervals 37.5-160 nm⁻¹ and 15.5-161.9 nm⁻¹ for Fe₃O₄ and Ni as test samples.

In order to obtain the RSF we use equation (4). The mean Fe-O distances of the first and the second coordination shell for standard sample at room temperature are close to values of $R_1 = 0.189$ nm and $R_2 = 0.209$ nm. By taking into account this very small difference between R_1 , R_2 and the discrimination steps, Δk and Δr of $\chi(k)$ and $\Phi(r)$ functions given by relation (5), we conclude that it is not possible to obtain a reliable resolution for the RSF. This means that the first and second shells are overlapped or only partial separated.

To avoid this disadvantage we developed the Filon algorithm for calculation of the Fourier transform described in relations (7-8). Based on this procedure the Fourier transforms of $k^3\chi(k)WF(k)$ performed in the interval 0.01-0.5 nm, are shown in figure 3 for standard Fe₃O₄ powder. Each peak from $|\Phi(r)|$ is shifted from the true distance due to the phase shift function that is included in the EXAFS signal. In the standard sample, the iron ions [Fe³⁺] and [Fe²⁺, Fe³⁺] from tetrahedral and octahedral structure are surrounded by four and six oxygen anions [O²⁻], respectively. In the EXAFS measured spectra these three contributions are averaged.

By analyzing figure 3 we can observe the advantages of Filon quadrature in comparison with the fast Fourier transform algorithm. The peaks associated with the coordination shells have a much better resolution than FFT algorithm. Another important advantage consists in the large number of point pairs for each peak. This result is very important, for statistical reasons, in the numerical analysis of the coordination number and the radius values of the coordination shells based on the inverse Fourier transform technique.

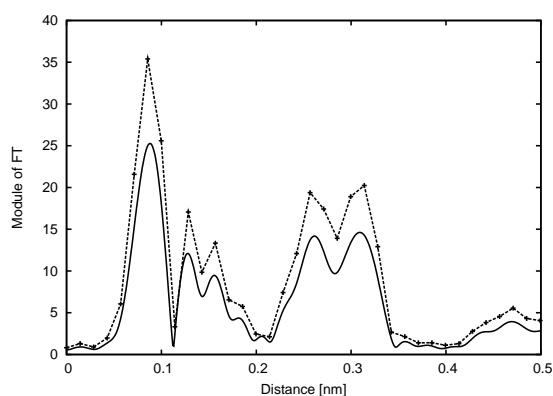


Figure 3. The Fourier transforms of the EXAFS spectra of Fe₃O₄ system (Filon quadrature -solid line, FFT algorithm - dashed line and +).

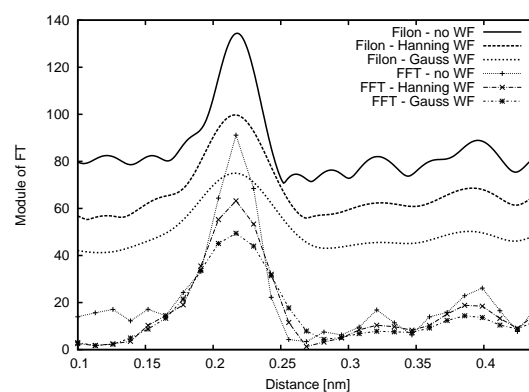


Figure 4. The Fourier transforms of the EXAFS spectra of supported Ni catalyst calculated by Filon quadrature and FFT algorithm.

The Fast Fourier transform method gives poor results when analyzing the close coordination shells because the peaks of the radial structure function from figure 3 have a poor resolution. Therefore they cannot be used in the calculation of the local structure parameters for systems that have close coordination shells. They contain one or more types of atoms distributed at two or more unique distances differing by 0.05 nm or less. Using Filon quadrature we obtained for the first and second coordination shells $N_1 = 3.11 \pm 0.009$ atoms, $r_1 = 0.189 \pm 0.001$ nm and $N_2 = 5.15 \pm 0.01$ atoms, $r_2 = 0.209 \pm 0.001$ nm, respectively. Generally speaking, such subshells are not resolved in the fast Fourier transform of the EXAFS spectra and can not be well analyzed by Fourier filtering technique. Other methods such as the regularization and the beat methods [12-14] in combination with the fast Fourier

transform of RSF are reported in literature. The results based on the last methods are more or less reliable.

Figure 4 shows the radial distribution function for Ni supported on Cr₂O₃ nanocrystallites calculated by both Filon quadrature and fast Fourier transform algorithms. Because the first and the second coordination shells are not close, $R_1 = 0.2491$ nm and $R_2 = 0.3524$ nm, they can be well separated by both algorithms. By using the similar procedure for the local structural parameters we obtained $N_1 = 9.32 \pm 0.11$ atoms, $r_1 = 0.25 \pm 0.06$ nm, $N_2 = 4.46 \pm 0.02$ atoms, $r_2 = 0.352 \pm 0.01$ nm, respectively. The meaning of the window function for each algorithm is also presented. Various types of window functions such as Hanning or Gaussian reduce the spurious errors due to integral truncation but they involve a broadening for each contribution.

5. Conclusions

In the present contribution we showed how various Fourier transform algorithms with their specific advantages apply to EXAFS analysis and what extra information can they add to understanding the nanostructure of the magnetite and supported nickel catalysts. The following conclusions can be drawn from these studies: (i) Filon quadrature can be successfully used for determination the local structure of the close-shell systems as magnetite while the fast Fourier transform algorithm gives unreliable results for this case; (ii) the classical fast Fourier transform method gives good results when the investigated samples are not close-shell systems as supported metal catalysts.

References

- [1] Lytle W F, Sayers E D and Stern A E 1989 *Physica B* **158** 701
- [2] Stern A E 1988 *X-Ray Absorption: Principles, Applications, Techniques of EXAFS, SEXAFS and XANES* (New York:Wiley)
- [3] Sinfelt H J, Via H G and Lytle W F 1984 *Catal. Rev. Sci. Eng.* **26** 81
- [4] Chen X L, Liu T, Thurnauer C M, Csencsits R and Rajh T 2002 *J. Phys. Chem. B* **106** 8539
- [5] Turcu R, Darabont A I, Nan A, Aldea N, Macovei D, Bica D, Vekas L, Pana O, Soran L M, Koos A A and Biro P L 2006 *J. Optoelectron. Adv. Mater.* **8** 643
- [6] Aldea N, Gluhoi A, Marginean P, Cosma C and Yaning X 2000 *Spectrochim. Acta B* **55** 997
- [7] McKale G A, Veal W B, Paulikas P A, Chan K S and Knapp S G 1988 *J. Am. Chem. Soc.* **110** 3763
- [8] Brigham O E 1974 *The Fast Fourier Transform* (New Jersey: Prentice-Hall Inc.)
- [9] Walker S J 1997 *Fast Fourier Transform* (New York/London/Tokyo: CRC Boca Raton)
- [10] Abramowich M and Stegun A 1968 *Handbook of Mathematical Functions* (New York: Dover)
- [11] Aldea N and Indrea E 1990 *Comput. Phys. Commun.* **60** 145
- [12] Babanov Yu *et al* 2005 *Phys. Scr.* **T115** 194
- [13] Bayanov I B, Bunker G and Morrison I T 1966 *J. Synchrotron Rad.* **3** 120
- [14] Gurman J S 1995 *J. Synchrotron Rad.* **2** 56.